

# Neural network distillation of orbital dependent density functional theory

Matija Medvidović,<sup>1</sup> Jaylyn C. Umana,<sup>2,3,4</sup> Iman Ahmadabadi,<sup>5,2,6</sup>  
Domenico Di Sante,<sup>7</sup> Johannes Flick,<sup>3,4,2</sup> and Angel Rubio<sup>8,2,9</sup>

<sup>1</sup>*Institute for Theoretical Physics, ETH Zürich, CH-8093 Zürich, Switzerland\**

<sup>2</sup>*Center for Computational Quantum Physics, Flatiron Institute, 162 5th Avenue, New York, NY 10010, USA*

<sup>3</sup>*Department of Physics, City College of New York, New York, NY 10031, USA*

<sup>4</sup>*Department of Physics, The Graduate Center, City University of New York, New York, NY 10016, USA*

<sup>5</sup>*Joint Quantum Institute, NIST and University of Maryland, College Park, MD 20742, USA*

<sup>6</sup>*Department of Chemistry, Princeton University, Princeton, NJ 08544, USA*

<sup>7</sup>*Department of Physics and Astronomy, University of Bologna, 40127 Bologna, Italy*

<sup>8</sup>*Max Planck Institute for the Structure and Dynamics of Matter,  
Luruper Chaussee 149, 22761 Hamburg, Germany*

<sup>9</sup>*Initiative for Computational Catalysis, Flatiron Institute, 162 5th Avenue, New York, NY 10010, USA*

(Dated: October 23, 2024)

Density functional theory (DFT) offers a desirable balance between quantitative accuracy and computational efficiency in practical many-electron calculations. Its central component, the exchange-correlation energy functional, has been approximated with increasing levels of complexity ranging from strictly local approximations to nonlocal and orbital-dependent expressions with many tuned parameters. In this work, we formulate a general way of rewriting complex density functionals using deep neural networks in a way that allows for simplified computation of Kohn-Sham potentials as well as higher functional derivatives through automatic differentiation, enabling access to highly nonlinear response functions and forces. These goals are achieved by using a recently developed class of robust neural network models capable of modeling functionals, as opposed to functions, with explicitly enforced spatial symmetries. Functionals treated in this way are then called *global density approximations* and can be seamlessly integrated with existing DFT workflows. Tests are performed for a dataset featuring a large variety of molecular structures and popular meta-GGA density functionals, where we successfully eliminate orbital dependencies coming from the kinetic energy density, and discover a high degree of transferability to a variety of physical systems. The presented framework is general and could be extended to more complex orbital and energy dependent functionals as well as refined with specialized datasets.

**Introduction** – The many-electron problem has been central to quantum physics for decades. With exact solutions out of reach in most cases, different approximate methods have been used in their place, offering controlled tradeoffs between efficiency, accuracy, and applicability. Density functional theory (DFT) [1–5] should be contrasted with the accuracy of wavefunction methods such as full configuration interaction (FCI) [6], coupled cluster [7, 8], quantum Monte Carlo (QMC) [9–12] and Green’s function methods like dynamical mean field theory (DMFT) [13–18] due to its considerably lower computational cost while still capturing the essential physics in most cases. This feature often makes DFT the only method that can access many-electron physics at large scales becoming the method of choice in solid state physics, quantum chemistry, and material science [19].

While the existence of the exact energy functional mapping from the electron densities to energies has been proven [1], its explicit form remains unknown. Approximate forms of the exchange-correlation (XC) energy functional have been constructed at varying levels of complexity [2, 20–28]. More recently, expressive machine learning methods have been used to build representations of XC functionals from data [29–41], showing that achieving chemically accurate, efficient and transferable functionals is feasible, at least within a targeted domain.

In this paper, we propose a method of constructing fully machine-learned nonlocal XC functionals based on a novel neural-network architecture, reproducing known functionals with high accuracy. There are two benefits of constructing a neural-network copy of known functionals. Firstly, for meta-GGA functionals, we eliminate the orbital dependence of the kinetic contribution to the XC energy by directly controlling data generation and neural-network inputs during training. Secondly, higher-order functional derivatives of resulting XC functionals can easily be evaluated using automatic differentiation (AD) tools [42, 43]. We call this method the global density approximation (GDA).

The neural network model used in this work is built around recent progress in transformer models that have recently revolutionized natural language and image processing [44, 45]. We employ the linear version of the underlying attention mechanism [46–48] to customize the network architecture for functional learning while respecting underlying spatial symmetries.

**The GDA method** – Consider an isolated molecule with  $N$  electrons in an external potential  $v_{\text{ext}}(\mathbf{r})$ . We limit the discussion to isolated molecules in this letter but the discussion is equally applicable to solids and other quantum systems. A standard DFT calculation [3, 4, 49] outputs an approximation to the ground state density  $n_0$

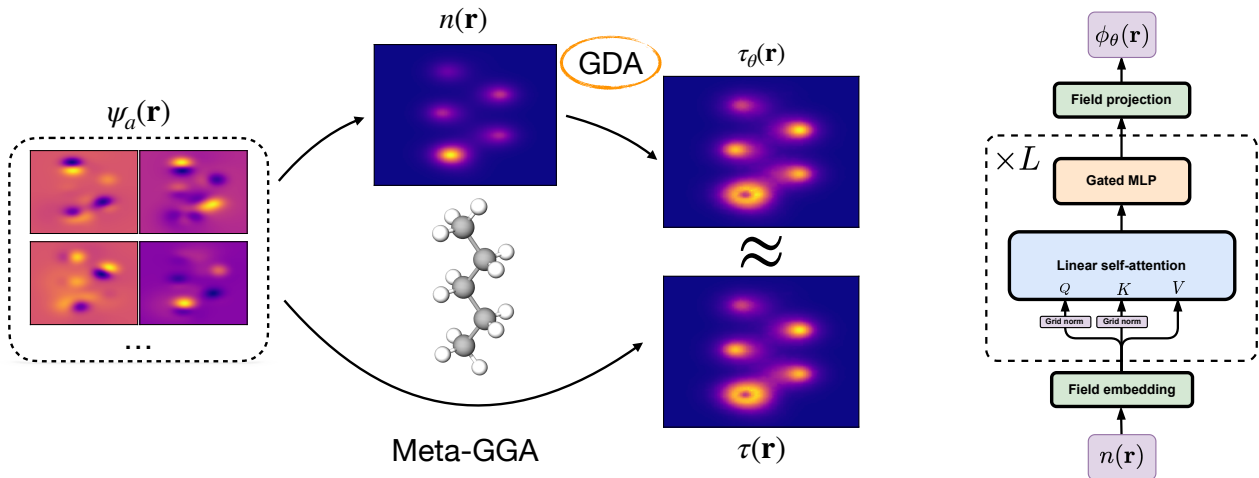


FIG. 1. A schematic representation of the global density approximation scheme. **Left:** The approximation scheme in which the kinetic energy density  $\tau$  is directly inferred from the density, eliminating the orbital dependence in all resulting functionals. **Right:** A diagrammatic representation of the internal connectivity of the GDA model. We use  $L = 3$  blocks and  $d = 128$  as the dimension of the internal field representation.

minimizing the total energy:  $n_0(\mathbf{r}) = \operatorname{argmin}_n E[n]$ . The total energy functional  $E[n]$  is commonly written as

$$E[n] = T[n] + E_{\text{ext}}[n] + E_H[n] + E_{\text{xc}}[n] \quad (1)$$

where the external contribution  $E_{\text{ext}}[n]$  captures the effects of  $v_{\text{ext}}(\mathbf{r})$  and the direct Hartree component  $E_H$  is directly computable given the density  $n(\mathbf{r})$ . We use atomic units throughout.

Successful evaluation Eq. 1 depends on approximating the unknown kinetic and exchange-correlation (XC) functionals,  $T[n]$  and  $E_{\text{xc}}[n]$ . The Kohn-Sham (KS) DFT [2] framework approximates the ground state density as induced by an effective system of non-interacting electrons,  $n(\mathbf{r}) = \sum_a n_a |\psi_a(\mathbf{r})|^2$ , where  $n_a$  is the occupation of the single-particle orbital  $\psi_a(\mathbf{r})$  with energies  $\epsilon_a$ . Crucially, orbitals also allow for an approximate treatment of the kinetic energy contribution as  $T = \int d^3\mathbf{r} \tau(\mathbf{r})$  with the kinetic energy density  $\tau$  given by

$$\tau(\mathbf{r}) = \frac{1}{2} \sum_a n_a |\nabla \psi_a(\mathbf{r})|^2. \quad (2)$$

For an overview of KS-DFT, we refer readers to the Supp. Mat. and Refs. [3, 4, 49–51].

After the desired XC functional has been specified, the constrained minimization of the total energy functional given in Eq. 1 can proceed, yielding Kohn-Sham equations [2] outlined in the Supp. Mat. These equations have to be solved in a self-consistent (SCF) manner, ensuring that  $n(\mathbf{r}) = \sum_a n_a |\psi_a(\mathbf{r})|^2$  holds at all times.

The exact energy functional is unknown. However, approximations with increasing levels of complexity have been ordered into the so-called *Jacob’s ladder* [20].

Higher rungs capture more details of local density neighborhoods at increased computational cost, starting with the local density approximations (LDA) which approximates electron XC effects as a uniform gas of interacting electrons of density  $n(\mathbf{r})$  [52]. While providing a good approximation for systems with slowly varying densities, it often lacks accuracy for molecular systems. This motivated the development of the second rung, the generalized gradient approximation (GGA) [24, 53], which includes  $\nabla n(\mathbf{r})$  as a local variable, offering better accuracy for a wider range of chemical systems. Further above in the ladder come the meta-GGA functionals [54–64], which capture more complex electronic interactions and offer improved accuracy for diverse systems, especially in terms of chemical reactivity and band gaps. These benefits come at the cost of having to include new local variables such as  $\tau(\mathbf{r})$  and its orbital dependence via Eq. 2.

Mathematically, the capacity to numerically solve the KS equations and access observables relies on our ability to approximate functional derivatives of the total energy in Eq. 1 during the SCF loop. In this letter, we propose an approximation to efficiently estimate functional derivatives of common meta-GGA density functionals by systematically removing orbital dependence. We do this by fitting them to expressive parameterized neural network models with restricted input variables. After capturing the target functional to a satisfactory degree, derivatives of the model can be efficiently calculated using automatic differentiation tools [42, 43, 65].

We rewrite the kinetic energy density as  $\tau \approx \tau_\theta[n]$ , a nonlocal functional captured by an expressive deep neural network [68–70] with  $\theta$  indicating a set of all free param-

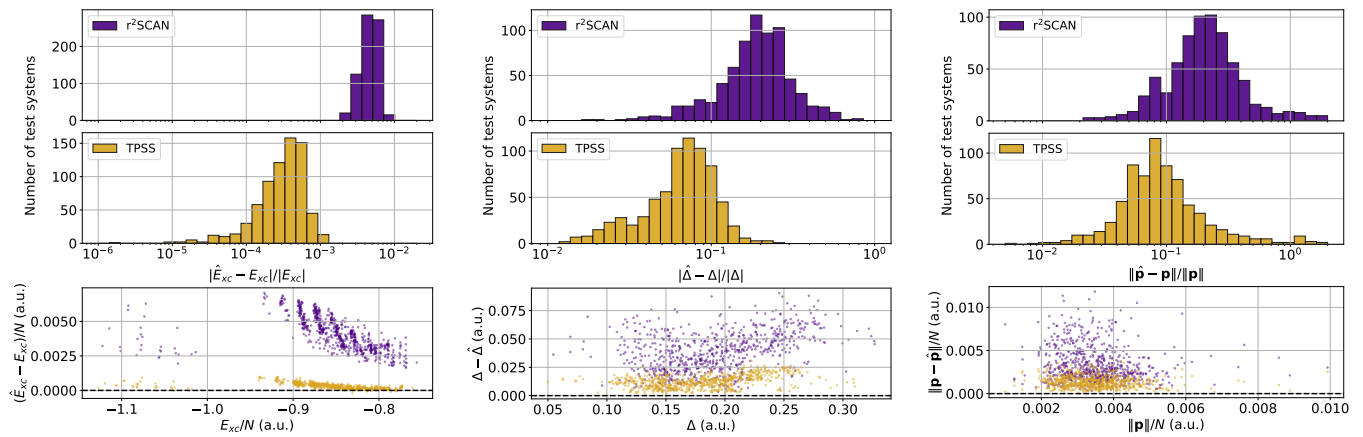


FIG. 2. Error distributions of observables obtained from first-principles calculations using the GDA approximation. The surrogate functional was tested on 717 test molecular systems withheld during training, a random selection of 10% of the QM7 [66, 67] dataset. **Left:** XC energy values. **Middle:** HOMO-LUMO gap values. **Right:** Total dipole moments.

eters in neural network sub-components (see Supp. Mat. for details). This approximation allows us to trivially rewrite any meta-GGA functional as

$$E_{xc}^{\text{GDA}}[n] = \int d^3\mathbf{r} n(\mathbf{r}) \varepsilon_{xc}(n(\mathbf{r}), \nabla n(\mathbf{r}), \tau_\theta[n](\mathbf{r})), \quad (3)$$

turning it into a nonlocal density functional.

**The neural network model** – In Eq. 3, we parametrize the kinetic energy density  $\tau_\theta[n]$  as a deep neural network, capable of approximating functionals in a controlled way while respecting underlying spatial symmetries. To introduce an additional useful inductive bias, we model the local dimensionless enhancement factor with a parametrized form  $\phi_\theta[n](\mathbf{r})$ , such that

$$\tau_\theta(\mathbf{r}) = \tau_W(\mathbf{r}) + e^{\phi_\theta(\mathbf{r})} (\tau_U(\mathbf{r}) + \eta \tau_W(\mathbf{r})) \quad (4)$$

is represented by a neural network with parameters  $\theta \in \mathbb{R}^P$ , based on a dimensionless kinetic energy indicator variable used in Ref. [62]. In Eq. 4,  $\tau_U = \frac{3}{10} (3\pi^2)^{2/3} n^{5/3}$  is the uniform electron gas kinetic energy,  $\tau_W = |\nabla n|^2 / 8n$  is the von Weizsäcker [71] kinetic functional and  $\eta = 10^{-3}$ , as defined in Ref. [62] and discussed in Supp. Mat.

Our architecture is similar to an encoder-only transformer [44] with linear attention modules [46, 47]. Attention layers were chosen because of the permutation equivariance property – permuting input values on the grid also permutes outputs in the same way, making this architecture well-suited for functional learning on grids.

We highlight two main differences in internal component design: a flexible density embedding layer, lifting the density into a high-dimensional representation while respecting underlying symmetries, and a specialized linear attention layers to directly operate on DFT grids equipped with custom normalization sub-components.

Local molecular densities can vary several orders of magnitude, depending on proximity to nuclei. To nor-

malize density variations, we construct the following dimensionless  $d$ -component input field:

$$\phi(\mathbf{r}) = \overline{\ln n(\mathbf{r})} \mathbf{e}_n + \overline{\ln |\nabla n(\mathbf{r})|^2} \mathbf{e}_\gamma, \quad (5)$$

where  $\mathbf{e}_n, \mathbf{e}_\gamma \in \mathbb{R}^d$  are trainable vectors and  $\overline{f(\mathbf{r})}$  indicates subtracting the mean and dividing by the standard deviation of  $f(\mathbf{r})$  with respect to the distribution  $n(\mathbf{r})/N$ . Input  $\phi$  values are updated by subsequent network layers.

To make  $\phi_\theta$  invariant with respect to translations and rotations of input coordinates we use a symmetry-aware *positional encoding* sub-layer. All computations are performed in a coordinate system where the mean value (dipole moment) of the density distribution  $n(\mathbf{r})/N$  vanishes and the covariance matrix is diagonal. This choice eliminates the special Euclidean symmetries in SE(3), determining the resulting computational coordinate values up to molecular point-group symmetries.

The coordinates are then lifted to a  $d$ -dimensional representation using random Fourier features (RFF) [72–74] combined with the density embedding of Eq. 5 using a gating mechanism described in Ref. [75]. The lifted density representation is then processed by a sequence of  $L$  blocks. One GDA block is defined as a stack of self-attention (SA) and gated multi-layer perceptron (MLP) layers [75] with SiLU activations [76]. After  $L$  blocks, one final projection layer consisting of an elementwise gated MLP is applied, projecting the point-wise embeddings into a single real number per coordinate  $\mathbf{r}$ , which we then interpret as the final value of the field  $\phi = \phi_\theta[n](\mathbf{r})$  in Eq. 4. We refer the reader to Fig. 1 for an overview of the internal connectivity and the Supp. Mat. for numerical and technical details.

The nonlocality in the GDA model is captured by the linear attention layer [46, 47]. The input field  $\phi$  is transformed as:

$$\phi'(\mathbf{r}) = \int d^3\mathbf{r}' n(\mathbf{r}') (Q(\mathbf{r}) \cdot K(\mathbf{r}')) V(\mathbf{r}') \quad (6)$$

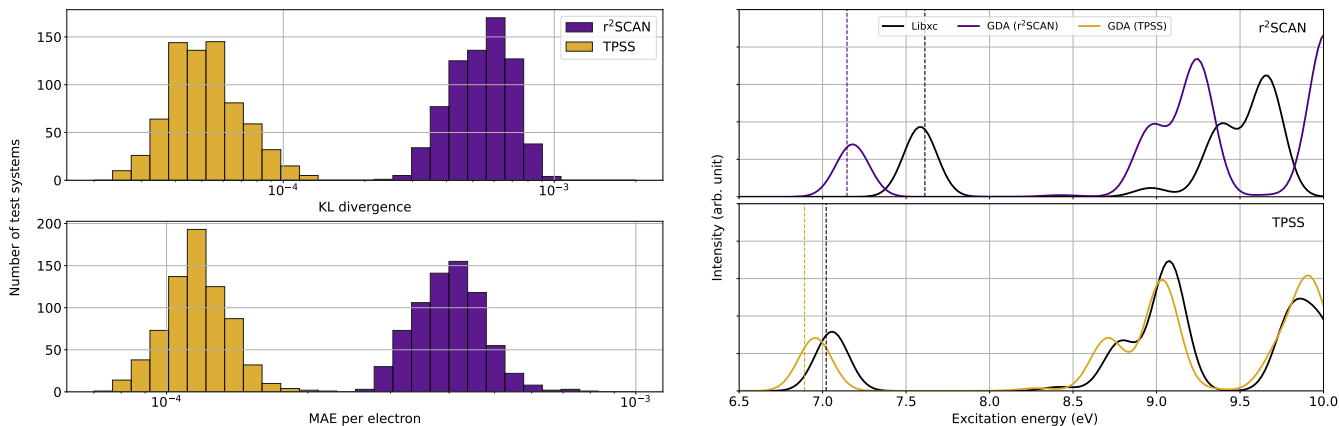


FIG. 3. Comparison of first-principles densities calculated using independent KS-DFT calculations and an example linear-response calculation of dimethyl ether ( $\text{CH}_3\text{OCH}_3$ ) spectra using TD-DFT where the predicted KS gaps are indicated by vertical lines in the same style as the corresponding spectra.

where  $Q_i(\mathbf{r}), K_i(\mathbf{r}), V_i(\mathbf{r})$  are the *query*, *key* and *value* parametrized local projections of the input field:  $\sum_k W_{ik}^{Q,K,V} \phi_k(\mathbf{r})$ . Furthermore, we employ rotary positional encoding (RoPE) [47, 48] independently for each block to ensure that the product  $Q(\mathbf{r}) \cdot K(\mathbf{r}') = \mathcal{K}(\mathbf{r} - \mathbf{r}')$  depends only on the relative coordinate, parametrizing a flexible continuous convolutional kernel. Details are given in the Supp. Mat.

The GDA model  $\phi_\theta$  is trained using gradient-based optimization of parameters  $\theta$  using the RAdam optimizer [77–79] and the gradients [80] of the scalar cost function

$$\mathcal{C}(\theta) = \frac{\|\phi_\theta - \phi_0\|_G^2}{\|\phi_0\|_G^2} + \lambda \frac{\|\mathcal{T} - \mathcal{T}_0\|_F^2}{\|\mathcal{T}_0\|_F^2} \quad (7)$$

consisting of two terms. The first term is the scaled mean squared error (MSE) for  $\phi$  itself where the unweighted grid norm  $\|f\|_G^2 = \sum_i f(\mathbf{r}_i)^2$  is defined over all DFT grid points  $\{\mathbf{r}_1, \dots, \mathbf{r}_{N_g}\}$ , where  $\phi_0(\mathbf{r})$  is evaluated from pre-calculated  $\tau$  values in the dataset, by inverting Eq. 4. The second term in Eq. 7 enforces the correct predicted kinetic energy matrix  $\mathcal{T}$  in the KS orbital basis, which can be easily predicted from the one-body electronic density matrix  $\Gamma$  as

$$\mathcal{T}_{ab} = \sum_{\mu\nu} C_{\mu a} C_{\nu b} \frac{\partial T[n]}{\partial \Gamma_{\mu\nu}} \quad (8)$$

by using standard AD routines and the LCAO expansion coefficients  $C_{\mu a}$ , see Supp. Mat. Reference values  $\mathcal{T}_0$  can be precalculated as  $\mathcal{T}_{0,ab} = \frac{1}{2} \int d^3\mathbf{r} \nabla \psi_a \cdot \nabla \psi_b$  from easily accessible basis set integrals [81, 82].

Including the second term in the cost function in Eq. 7 ensures that the kinetic contribution to the overall KS effective Hamiltonian  $H_{\text{eff}} = \partial E / \partial \Gamma$  is well approximated by the GDA surrogate functional when solving the KS equation  $C^\top H_{\text{eff}} C = \epsilon$ . We find that including such a

gradient cost term is key for making the resulting neural network functional converge in a practical DFT SCF calculation, allowing us to use it to obtain energies, orbitals, densities or observables from first principles, without ever referring to the parent functional. Similar regularization methods have been proposed in Refs. [38, 83].

**Results** – We examine GDA approximations to two prominent meta-GGA functionals:  $r^2\text{SCAN}$  [28, 59, 60, 62] and TPSS [54]. We use a single neural-network GDA model for evaluation of all molecules for all three functionals. Each functional is tested in both ground state KS-DFT and linear response TD-DFT calculations. The architecture outlined in Fig. 1 with  $L = 3$  blocks and the embedding dimension of  $d = 128$  is used and optimized using  $\lambda = 1$  in Eq. 7. Molecular geometries from the QM7 [66, 67] dataset are used, consisting of 7165 organic molecules of up to 23 atoms, and featuring a large variety of molecular structures such as double and triple bonds, cycles, carboxy, cyanide, amide, alcohol and epoxy. Corresponding KS-DFT calculations were done using the  $r^2\text{SCAN}$  functional to obtain input densities and target  $\tau$  values.

We independently calculate and compare several physical observables – the total energy, the molecular dipole moment, the KS HOMO-LUMO gap, and the self-consistent density itself. Error distributions are shown on Fig. 2, demonstrating that the resulting surrogate GGA functionals converge to physical results independently from the source meta-GGA functional, using only density inputs as shown in Eq. 3.

The GDA functional is able to accurately predict XC energies and potentials over a large range of diverse test molecules, eliminating orbital dependence from input functionals. Gap values are predicted within 10% for TPSS with higher errors in  $r^2\text{SCAN}$  calculations where GDA approximations tend to over-estimate the gap. A similar trend persists with dipole moments, demonstrat-

ing qualitative accuracy. Since all of the results have been obtained with a single transferable neural-network model, the GDA approximation scheme eliminates the need to train multiple models for de-orbitalizing different XC functionals and can serve as a starting point for more fine-tuned approximations. Furthermore, we speculate that such broad generalization for larger models trained on more diverse datasets can be used to train foundation functionals to then fine-tune on downstream problems with limited data.

As a direct global divergence measure between two densities, we consider the Kullback-Liebler (KL) divergence [84]  $D_{\text{KL}}(n \parallel \hat{n}) = \frac{1}{N} \int d^3\mathbf{r} n(\mathbf{r}) \ln \frac{n(\mathbf{r})}{\hat{n}(\mathbf{r})}$  commonly used in statistical literature, where  $\hat{n}$  is the density obtained by independent SCF convergence using the GDA approximation of the original functional. In addition, we also compare direct mean absolute errors (MAEs) of density values defined as  $D_{\text{MAE}}(n, \hat{n}) = \frac{1}{N} \int d^3\mathbf{r} |n(\mathbf{r}) - \hat{n}(\mathbf{r})|$ . In all cases the trained model produces a good approximation to the ground-state density indicating good transferability, as can be seen on the left panel of Fig. 3. We see that TPSS densities are reproduced more accurately indicating that the generated dataset based on QM7 is better suited to some typical densities encountered with that functional. A more expansive dataset with more diverse densities and geometries is likely to close the gap in Fig. 3.

To showcase the performance of the GDA in the excited state regime, we present a minimal but relevant demonstration in the right panel of Fig. 3. Here, we simulate absorption spectra via linear response for a single test molecule, chosen for size and proximity to the dataset. We compare spectra generated using the GDA model against the parent functionals accessed through the Libxc [85, 86] library. Calculations are carried out in the Casida TD-DFT [87] formalism for 100 excited states, and we focus on a low energy range to highlight the ability of our model to replicate physically meaningful features before the ionization threshold [88, 89] in a similar fashion to the original functional. Unsurprisingly, the GDA most closely captures the behavior of TPSS. The GDA model has a higher error in r<sup>2</sup>SCAN for this particular case with the expectation that predictions can be improved by using larger GDA neural networks trained on more diverse density inputs.

**Conclusions and outlook** – We introduce a new class of approximations, enabling first-principles replacement of orbital-dependent meta-GGA functionals. Using these approximations, arbitrary derivatives of source functionals can be constructed, enabling access to new results and phenomena (e.g. highly nonlinear responses). As a proof of principle, this approximation is accurate and resource-efficient with a high degree of transferability between different functionals and physical systems. In addition, our GDA approximation scheme formally en-

ables the use of orbital-free DFT (OF-DFT) calculations at the meta-GGA level of theory. However robust OF-DFT solvers for Gaussian-type basis sets are still an active area of research with experimental support for non-local functionals at best. Therefore, extending the GDA approximation to OF-DFT is left for future research.

More general orbital-dependent functionals have shown great potential in overcoming the limitations of their pure density functionals. Hybrid functionals, such as B3LYP, HSE and PBE0 [25, 90, 91], which combine GGA functionals with a fraction of orbital-dependent exact exchange, have achieved superior accuracy in predicting molecular geometries, reaction barriers, and electronic properties. The GDA formalism allows reformulating orbital-dependent functionals as pure but nonlocal density functionals, offering a promising direction to bridge the gap between *pure* DFT and the quantum chemical accuracy.

**Software and simulations** – All DFT simulations were performed using a custom interface between the PySCF [81, 82] library and PyTorch [65, 80], used for automatic generation of XC potentials for KS-DFT calculations and kernels for linear-response TD-DFT calculations. All calculations were performed using the cc-pVDZ basis set at grid level 1 in PySCF. Convergence tolerance was set to 10<sup>-6</sup> Ha. Code needed to reproduce results in this work or experiment with new results has been open-sourced and can be found at the following URL: <https://github.com/Matematija/global-density-approximation>.

**Acknowledgements** – M. M. and J. C. U. acknowledge support from the CCQ graduate fellowship in computational quantum physics. The Flatiron Institute is a division of the Simons Foundation.

---

\* [mmedvidovic@ethz.ch](mailto:mmedvidovic@ethz.ch)

- [1] P. Hohenberg and W. Kohn, Physical Review **136**, B864 (1964), ISSN 0031-899X, URL <https://link.aps.org/doi/10.1103/PhysRev.136.B864>.
- [2] W. Kohn and L. J. Sham, Physical Review **140**, A1133 (1965), ISSN 0031-899X, URL <https://link.aps.org/doi/10.1103/PhysRev.140.A1133>.
- [3] M. A. Marques, C. A. Ullrich, F. Nogueira, A. Rubio, K. Burke, and E. K. U. Gross, eds., *Time-Dependent Density Functional Theory*, vol. 706 (Springer Berlin Heidelberg, Berlin, Heidelberg, 2006), ISBN 978-3-540-35422-2, series Title: Lecture Notes in Physics, URL <http://link.springer.com/10.1007/b11767107>.
- [4] C. Fiolhais, F. Nogueira, M. A. L. Marques, R. Beig, B. G. Englert, U. Frisch, P. Hänggi, K. Hepp, W. Hillebrandt, D. Imboden, et al., eds., *A Primer in Density Functional Theory*, vol. 620 of *Lecture Notes in Physics* (Springer, Berlin, Heidelberg, 2003), ISBN 978-3-540-03083-6 978-3-540-37072-7, URL <http://link.springer.com/10.1007/3-540-37072-2>.
- [5] G. Onida, L. Reining, and A. Rubio, Reviews of Mod-

- ern Physics **74**, 601 (2002), publisher: American Physical Society, URL <https://link.aps.org/doi/10.1103/RevModPhys.74.601>.
- [6] J. A. Pople, M. Head-Gordon, and K. Raghavachari, The Journal of Chemical Physics **87**, 5968 (1987), ISSN 0021-9606, URL <https://doi.org/10.1063/1.453520>.
- [7] R. J. Bartlett and M. Musiał, Reviews of Modern Physics **79**, 291 (2007), ISSN 0034-6861, 1539-0756, URL <https://link.aps.org/doi/10.1103/RevModPhys.79.291>.
- [8] B. Jeziorski and H. J. Monkhorst, Phys. Rev. A **24**, 1668 (1981), publisher: American Physical Society, URL <https://link.aps.org/doi/10.1103/PhysRevA.24.1668>.
- [9] F. Becca and S. Sorella, *Quantum Monte Carlo Approaches for Correlated Systems* (Cambridge University Press, 2017), ISBN 978-1-107-12993-1, URL <https://www.cambridge.org/core/product/identifier/9781316417041/type/book>.
- [10] D. Wu, R. Rossi, F. Vicentini, N. Astrakhantsev, F. Becca, X. Cao, J. Carrasquilla, F. Ferrari, A. Georges, M. Hibat-Allah, et al. (2023), URL <http://arxiv.org/abs/2302.04919>.
- [11] M. Medvidović and J. Robledo Moreno, *Neural-network quantum states for many-body physics* (2024), URL <http://arxiv.org/abs/2402.11014>.
- [12] J. Lee, H. Q. Pham, and D. R. Reichman, Journal of Chemical Theory and Computation **18**, 7024 (2022), ISSN 1549-9618, 1549-9626, URL <https://pubs.acs.org/doi/10.1021/acs.jctc.2c00802>.
- [13] A. Georges and G. Kotliar, Phys. Rev. B **45**, 6479 (1992), publisher: American Physical Society, URL <https://link.aps.org/doi/10.1103/PhysRevB.45.6479>.
- [14] A. Georges, G. Kotliar, W. Krauth, and M. J. Rozenberg, Reviews of Modern Physics **68**, 13 (1996), ISSN 0034-6861, 1539-0756, URL <https://link.aps.org/doi/10.1103/RevModPhys.68.13>.
- [15] L. Hedin, Physical Review **139**, A796 (1965), publisher: American Physical Society, URL <https://link.aps.org/doi/10.1103/PhysRev.139.A796>.
- [16] F. Aryasetiawan and O. Gunnarsson, Reports on Progress in Physics **61**, 237 (1998), ISSN 0034-4885, URL <https://dx.doi.org/10.1088/0034-4885/61/3/002>.
- [17] L. Reining, WIREs Computational Molecular Science **8**, e1344 (2018), ISSN 1759-0884, eprint: <https://onlinelibrary.wiley.com/doi/pdf/10.1002/wcms.1344>, URL <https://onlinelibrary.wiley.com/doi/abs/10.1002/wcms.1344>.
- [18] D. Golze, M. Dvorak, and P. Rinke, Frontiers in Chemistry **7**, 377 (2019), ISSN 2296-2646.
- [19] K. Burke, The Journal of Chemical Physics **136** (2012), ISSN 0021-9606, 1089-7690, publisher: AIP Publishing, URL <https://pubs.aip.org/jcp/article/136/15/150901/941589/Perspective-on-density-functional-theory>.
- [20] J. P. Perdew, in *AIP Conference Proceedings* (AIP, 2001), vol. 577, pp. 1–20, iSSN: 0094243X, URL <https://pubs.aip.org/aip/acp/article/577/1/1-20/573973>.
- [21] A. Seidl, A. Görling, P. Vogl, J. A. Majewski, and M. Levy, Phys. Rev. B **53**, 3764 (1996), publisher: American Physical Society, URL <https://link.aps.org/doi/10.1103/PhysRevB.53.3764>.
- [22] C. Lee, W. Yang, and R. G. Parr, Phys. Rev. B **37**, 785 (1988), publisher: American Physical Society, URL <https://link.aps.org/doi/10.1103/PhysRevB.37.785>.
- [23] A. D. Becke, The Journal of Chemical Physics **98**, 5648 (1993), ISSN 0021-9606, URL <https://doi.org/10.1063/1.464913>.
- [24] J. P. Perdew, K. Burke, and M. Ernzerhof, Physical Review Letters **77**, 3865 (1996), ISSN 0031-9007, URL <https://link.aps.org/doi/10.1103/PhysRevLett.77.3865>.
- [25] J. Heyd, G. E. Scuseria, and M. Ernzerhof, The Journal of Chemical Physics **118**, 8207 (2003), ISSN 0021-9606, URL <https://doi.org/10.1063/1.1564060>.
- [26] S. Grimme, Journal of Computational Chemistry **27**, 1787 (2006), URL <https://onlinelibrary.wiley.com/doi/abs/10.1002/jcc.20495>.
- [27] A. Tkatchenko and M. Scheffler, Phys. Rev. Lett. **102**, 073005 (2009), publisher: American Physical Society, URL <https://link.aps.org/doi/10.1103/PhysRevLett.102.073005>.
- [28] J. Sun, R. C. Remsing, Y. Zhang, Z. Sun, A. Ruzsinszky, H. Peng, Z. Yang, A. Paul, U. Waghmare, X. Wu, et al. (2015), arXiv: 1511.01089, URL <http://arxiv.org/abs/1511.01089>.
- [29] J. C. Snyder, M. Rupp, K. Hansen, K.-R. Müller, and K. Burke, Phys. Rev. Lett. **108**, 253002 (2012).
- [30] M. Bogojeski, L. Vogt-Maranto, M. E. Tuckerman, K.-R. Müller, and K. Burke, Nature communications **11**, 5223 (2020), publisher: Nature Publishing Group UK London, URL <https://www.nature.com/articles/s41467-020-19093-1>.
- [31] K. Bystrom and B. Kozinsky, Journal of Chemical Theory and Computation **18**, 2180 (2022), URL <https://doi.org/10.1021/acs.jctc.1c00904>.
- [32] S. Dick and M. Fernandez-Serra, Nature Communications **11**, 3509 (2020), ISSN 2041-1723, URL <https://www.nature.com/articles/s41467-020-17265-7>.
- [33] X. Lei and A. J. Medford, Phys. Rev. Mater. **3**, 063801 (2019), publisher: American Physical Society, URL <https://link.aps.org/doi/10.1103/PhysRevMaterials.3.063801>.
- [34] Y. Chen, L. Zhang, H. Wang, and W. E, Journal of Chemical Theory and Computation **17**, 170 (2021), ISSN 1549-9618, 1549-9626, URL <https://pubs.acs.org/doi/10.1021/acs.jctc.0c00872>.
- [35] R. Nagai, R. Akashi, and O. Sugino, npj Computational Materials **6**, 43 (2020), ISSN 2057-3960.
- [36] P. A. M. Casares, J. S. Baker, M. Medvidović, R. d. Reis, and J. M. Arrazola, The Journal of Chemical Physics **160**, 062501 (2024), ISSN 0021-9606, URL <https://doi.org/10.1063/5.0181037>.
- [37] B. G. Del Rio, B. Phan, and R. Ramprasad, npj Computational Materials **9**, 158 (2023), ISSN 2057-3960, URL <https://www.nature.com/articles/s41524-023-01115-3>.
- [38] J. Kirkpatrick, B. McMorrow, D. H. P. Turban, A. L. Gaunt, J. S. Spencer, A. G. D. G. Matthews, A. Obika, L. Thiry, M. Fortunato, D. Pfau, et al., Science **374**, 1385 (2021), ISSN 0036-8075.
- [39] J. T. Margraf and K. Reuter, Nature communications **12**, 344 (2021), URL <https://www.nature.com/articles/s41467-020-20471-y>.
- [40] K. Bystrom and B. Kozinsky, arXiv preprint arXiv:2303.00682 (2023), URL <https://arxiv.org/abs/2303.00682>.
- [41] K. Bystrom, S. Falletta, and B. Kozinsky, arXiv preprint

- arXiv:2403.17002 (2024), URL <https://arxiv.org/abs/2303.00682>.
- [42] C. C. Margossian, WIREs Data Mining and Knowledge Discovery **9** (2019), ISSN 1942-4787, URL <https://wires.onlinelibrary.wiley.com/doi/10.1002/widm.1305>.
- [43] A. G. Baydin, B. A. Pearlmutter, A. A. Radul, and J. M. Siskind, Journal of Machine Learning Research **18**, 1 (2018), URL <http://jmlr.org/papers/v18/17-468.html>.
- [44] A. Vaswani, N. Shazeer, N. Parmar, J. Uszkoreit, L. Jones, A. N. Gomez, L. Kaiser, and I. Polosukhin (2017), arXiv: 1706.03762, URL <http://arxiv.org/abs/1706.03762>.
- [45] A. Dosovitskiy, L. Beyer, A. Kolesnikov, D. Weissenborn, X. Zhai, T. Unterthiner, M. Dehghani, M. Minderer, G. Heigold, S. Gelly, et al. (2020), arXiv: 2010.11929, URL <http://arxiv.org/abs/2010.11929>.
- [46] S. Cao, *Choose a Transformer: Fourier or Galerkin* (2021), arXiv:2105.14995 [cs, math], URL <http://arxiv.org/abs/2105.14995>.
- [47] Z. Li, K. Meidani, and A. B. Farimani, *Transformer for Partial Differential Equations' Operator Learning* (2023), arXiv:2205.13671 [cs], URL <http://arxiv.org/abs/2205.13671>.
- [48] J. Su, Y. Lu, S. Pan, A. Murtadha, B. Wen, and Y. Liu, *RoFormer: Enhanced Transformer with Rotary Position Embedding* (2023), arXiv:2104.09864 [cs], URL <http://arxiv.org/abs/2104.09864>.
- [49] R. M. Martin, *Electronic structure: basic theory and practical methods* (Cambridge university press, 2020).
- [50] R. O. Jones, Rev. Mod. Phys. **87**, 897 (2015), publisher: American Physical Society, URL <https://link.aps.org/doi/10.1103/RevModPhys.87.897>.
- [51] S. Kümmel and L. Kronik, Rev. Mod. Phys. **80**, 3 (2008), publisher: American Physical Society, URL <https://link.aps.org/doi/10.1103/RevModPhys.80.3>.
- [52] J. P. Perdew and A. Zunger, Physical Review B **23**, 5048 (1981), ISSN 0163-1829, URL <https://link.aps.org/doi/10.1103/PhysRevB.23.5048>.
- [53] D. C. Langreth and M. Mehl, Physical Review B **28**, 1809 (1983), URL <https://journals.aps.org/prb/abstract/10.1103/PhysRevB.28.1809>.
- [54] J. Tao, J. P. Perdew, V. N. Staroverov, and G. E. Scuseria, Physical Review Letters **91**, 146401 (2003), ISSN 0031-9007, 1079-7114, URL <https://link.aps.org/doi/10.1103/PhysRevLett.91.146401>.
- [55] J. P. Perdew, A. Ruzsinszky, G. I. Csonka, L. A. Constantin, and J. Sun, Physical Review Letters **103**, 026403 (2009), URL <https://journals.aps.org/prl/abstract/10.1103/PhysRevLett.103.026403>.
- [56] Y. Zhao and D. G. Truhlar, The Journal of chemical physics **125** (2006), URL <https://pubs.aip.org/aip/jcp/article-abstract/125/19/194101/566338/A-new-local-density-functional-for-main-group?redirectedFrom=fulltext>.
- [57] J. Sun, B. Xiao, and A. Ruzsinszky, The Journal of chemical physics **137** (2012), URL <https://pubs.aip.org/aip/jcp/article/137/5/051101/671610>.
- [58] J. Sun, R. Haunschild, B. Xiao, I. W. Bulik, G. E. Scuseria, and J. P. Perdew, The Journal of chemical physics **138** (2013), URL <https://pubs.aip.org/aip/jcp/article-abstract/138/4/044113/193378/Semilocal-and-hybrid-meta-generalized-gradient?redirectedFrom=fulltext>.
- [59] J. Sun, A. Ruzsinszky, and J. P. Perdew, Physical review letters **115**, 036402 (2015), URL <https://journals.aps.org/prl/abstract/10.1103/PhysRevLett.115.036402>.
- [60] J. Sun, R. C. Remsing, Y. Zhang, Z. Sun, A. Ruzsinszky, H. Peng, Z. Yang, A. Paul, U. Waghmare, X. Wu, et al., Nature chemistry **8**, 831 (2016), publisher: Nature Publishing Group UK London, URL <https://www.nature.com/articles/nchem.2535>.
- [61] A. P. Bartók and J. R. Yates, The Journal of chemical physics **150** (2019), URL <https://pubs.aip.org/aip/jcp/article/150/16/161101/198173>.
- [62] J. W. Furness, A. D. Kaplan, J. Ning, J. P. Perdew, and J. Sun, The Journal of Physical Chemistry Letters **11**, 8208 (2020), ISSN 1948-7185, 1948-7185, URL <https://pubs.acs.org/doi/10.1021/acs.jpcllett.0c02405>.
- [63] A. D. Becke and E. R. Johnson, The Journal of chemical physics **124** (2006), URL <https://pubs.aip.org/aip/jcp/article-abstract/124/22/221101/920551/A-simple-effective-potential-for-exchange?redirectedFrom=fulltext>.
- [64] F. Tran and P. Blaha, Physical review letters **102**, 226401 (2009), URL <https://journals.aps.org/prl/abstract/10.1103/PhysRevLett.102.226401>.
- [65] A. Paszke, S. Gross, S. Chintala, G. Chanan, E. Yang, Z. DeVito, Z. Lin, A. Desmaison, L. Antiga, and A. Lerer, in *NIPS 2017 Workshop Autodiff Decision Program Chairs* (2017), iSSN: 01635778.
- [66] L. C. Blum and J.-L. Raymond, Journal of the American Chemical Society **131**, 8732 (2009), ISSN 0002-7863, 1520-5126, URL <https://pubs.acs.org/doi/10.1021/ja902302h>.
- [67] M. Rupp, A. Tkatchenko, K.-R. Müller, and O. A. Von Lilienfeld, Physical Review Letters **108**, 058301 (2012), ISSN 0031-9007, 1079-7114, URL <https://link.aps.org/doi/10.1103/PhysRevLett.108.058301>.
- [68] Y. LeCun, Y. Bengio, and G. Hinton, Nature **521**, 436 (2015), ISSN 1476-4687, publisher: Nature Publishing Group, URL <http://www.ncbi.nlm.nih.gov/pubmed/26017442>.
- [69] I. Goodfellow, Y. Bengio, and A. Courville, *Deep Learning* (MIT Press, 2016), URL <http://www.deeplearningbook.org>.
- [70] A. Dawid, J. Arnold, B. Requena, A. Gresch, M. Płodzień, K. Donatella, K. A. Nicoli, P. Stornati, R. Koch, M. Büttner, et al. (2022), arXiv: 2204.04198, URL <http://arxiv.org/abs/2204.04198>.
- [71] C. F. V. Weizsäcker, Zeitschrift für Physik **96**, 431 (1935), ISSN 1434-6001, 1434-601X, URL <http://link.springer.com/10.1007/BF01337700>.
- [72] A. Rahimi and B. Recht, in *Advances in Neural Information Processing Systems*, edited by J. Platt, D. Koller, Y. Singer, and S. Roweis (Curran Associates, Inc., 2007), vol. 20, URL [https://proceedings.neurips.cc/paper\\_files/paper/2007/file/013a006f03dbc5392effeb8f18fda755-Paper.pdf](https://proceedings.neurips.cc/paper_files/paper/2007/file/013a006f03dbc5392effeb8f18fda755-Paper.pdf).
- [73] M. Tancik, P. P. Srinivasan, B. Mildenhall, S. Fridovich-Keil, N. Raghavan, U. Singhal, R. Ramamoorthi, J. T. Barron, and R. Ng (2020), arXiv: 2006.10739, URL <http://arxiv.org/abs/2006.10739>.
- [74] Y. Li, S. Si, G. Li, C.-J. Hsieh, and S. Bengio (2021), arXiv: 2106.02795, URL <http://arxiv.org/abs/2106.02795>.

- [75] N. Shazeer, *GLU Variants Improve Transformer* (2020), URL <https://arxiv.org/abs/2002.05202v1>.
- [76] S. Elfwing, E. Uchibe, and K. Doya (2017), arXiv: 1702.03118, URL <http://arxiv.org/abs/1702.03118>.
- [77] L. Liu, H. Jiang, P. He, W. Chen, X. Liu, J. Gao, and J. Han (2019), arXiv: 1908.03265, URL <http://arxiv.org/abs/1908.03265>.
- [78] D. P. Kingma and J. L. Ba, in *3rd International Conference on Learning Representations, ICLR 2015 - Conference Track Proceedings* (International Conference on Learning Representations, ICLR, 2015).
- [79] I. Loshchilov and F. Hutter, CoRR **abs/1711.05101** (2017), arXiv: 1711.05101, URL <http://arxiv.org/abs/1711.05101>.
- [80] A. Paszke, S. Gross, F. Massa, A. Lerer, J. Bradbury, G. Chanan, T. Killeen, Z. Lin, N. Gimelshein, L. Antiga, et al., *Advances in Neural Information Processing Systems* **32** (2019), arXiv: 1912.01703, URL <http://arxiv.org/abs/1912.01703>.
- [81] Q. Sun, T. C. Berkelbach, N. S. Blunt, G. H. Booth, S. Guo, Z. Li, J. Liu, J. D. McClain, E. R. Sayfutyarova, S. Sharma, et al., *WIREs Computational Molecular Science* **8**, e1340 (2018), URL <https://wires.onlinelibrary.wiley.com/doi/abs/10.1002/wcms.1340>.
- [82] Q. Sun, X. Zhang, S. Banerjee, P. Bao, M. Barbry, N. S. Blunt, N. A. Bogdanov, G. H. Booth, J. Chen, Z.-H. Cui, et al., *The Journal of Chemical Physics* **153**, 024109 (2020), ISSN 0021-9606, URL <https://doi.org/10.1063/5.0006074>.
- [83] P. d. Mazo-Sevillano and J. Hermann, *The Journal of Chemical Physics* **159** (2023), ISSN 0021-9606, URL <https://doi.org/10.1063/5.0166432>.
- [84] S. Kullback and R. A. Leibler, *The Annals of Mathematical Statistics* **22**, 79 (1951), ISSN 0003-4851, URL <http://projecteuclid.org/euclid.aoms/1177729694>.
- [85] M. A. Marques, M. J. Oliveira, and T. Burnus, *Computer physics communications* **183**, 2272 (2012).
- [86] S. Lehtola, C. Steigemann, M. J. Oliveira, and M. A. Marques, *SoftwareX* **7**, 1 (2018).
- [87] M. E. Casida, in *Recent Advances In Density Functional Methods: (Part I)* (World Scientific, 1995), pp. 155–192.
- [88] W.-C. Tam and C. Brion, *Journal of Electron Spectroscopy and Related Phenomena* **3**, 263 (1974).
- [89] P. Linstrom, W. Mallard, et al., *NIST Chemistry Web-Book* p. 20899 (2018).
- [90] P. J. Stephens, F. J. Devlin, C. F. Chabalowski, and M. J. Frisch, *The Journal of physical chemistry* **98**, 11623 (1994), URL <https://pubs.acs.org/doi/abs/10.1021/j100096a001>.
- [91] C. Adamo and V. Barone, *The Journal of chemical physics* **110**, 6158 (1999), URL <https://doi.org/10.1063/1.478522>.



# Neural network distillation of orbital dependent density functional theory

## Supplementary Material

Matija Medvidović,<sup>1</sup> Jaylyn C. Umana,<sup>2,3,4</sup> Iman Ahmadabadi,<sup>5,2,6</sup>  
Domenico Di Sante,<sup>7</sup> Johannes Flick,<sup>3,4,2</sup> and Angel Rubio<sup>8,2,9</sup>

<sup>1</sup>*Institute for Theoretical Physics, ETH Zürich, CH-8093 Zürich, Switzerland\**

<sup>2</sup>*Center for Computational Quantum Physics, Flatiron Institute, 162 5th Avenue, New York, NY 10010, USA*

<sup>3</sup>*Department of Physics, City College of New York, New York, NY 10031, USA*

<sup>4</sup>*Department of Physics, The Graduate Center, City University of New York, New York, NY 10016, USA*

<sup>5</sup>*Joint Quantum Institute, NIST and University of Maryland, College Park, MD 20742, USA*

<sup>6</sup>*Department of Chemistry, Princeton University, Princeton, NJ 08544, USA*

<sup>7</sup>*Department of Physics and Astronomy, University of Bologna, 40127 Bologna, Italy*

<sup>8</sup>*Max Planck Institute for the Structure and Dynamics of Matter,  
Luruper Chaussee 149, 22761 Hamburg, Germany*

<sup>9</sup>*Initiative for Computational Catalysis, Flatiron Institute, 162 5th Avenue, New York, NY 10010, USA*

(Dated: October 23, 2024)

### NEURAL NETWORK ARCHITECTURE

#### Linear attention layers as continuous convolutions

We consider input data in a point cloud format of density values with coordinates  $\mathbf{r}_i$ , density values  $n_i = n(\mathbf{r}_i)$  and quadrature weights  $w_i$  where  $i = 1, \dots, N_g$  indexes the cloud in arbitrary order. Functional inputs in this form are general and can be readily extracted from modern quantum chemistry software packages. This enables us to approximate integrals of sufficiently well-behaved functions as:

$$\int d^3\mathbf{r} f(\mathbf{r}) \approx \sum_i w_i f(\mathbf{r}_i). \quad (1)$$

Global density approximations rely on the linear attention [1] mechanism for propagating information between local density values. In purely mathematical terms, the linear self-attention operation used in this work can be seen as a discretization of an integral transform with a learnable kernel  $\mathcal{K}$ :

$$\phi'(\mathbf{r}) = \int d^3\mathbf{r}' n(\mathbf{r}') \mathcal{K}(\mathbf{r}, \mathbf{r}') \phi(\mathbf{r}') = \int d^3\mathbf{r}' n(\mathbf{r}') (Q(\mathbf{r}) \cdot K(\mathbf{r}')) V(\mathbf{r}') \quad (2)$$

where  $\mathcal{K}$  has been parameterized in factorized form in order to exploit the *kernel trick*.

In Eq. 2, we define the so-called queries, keys, and values  $Q, K, V \in \mathbb{R}^d$  as learnable local linear transformations of the input field  $\phi(\mathbf{r}) \in \mathbb{R}^d$ :

$$Q(\mathbf{r}) = W^Q \phi(\mathbf{r}), \quad K(\mathbf{r}) = W^K \phi(\mathbf{r}) \quad \text{and} \quad V(\mathbf{r}) = W^V \phi(\mathbf{r}). \quad (3)$$

The functional form of Eq. 2 should be contrasted with an equivalent definition of the standard `softmax` nonlinear attention [2, 3] kernel head

$$\mathcal{K}_{\text{sm}}(\mathbf{r}, \mathbf{r}') = \frac{e^{Q(\mathbf{r}) \cdot K(\mathbf{r}')}}{\int d^3\mathbf{r}'' e^{Q(\mathbf{r}) \cdot K(\mathbf{r}'')}} \quad (4)$$

where a similar kernel trick cannot be exploited.

Large integration grids of  $N_g > 10^6$  points are not uncommon in modern DFT calculations. Therefore, the naive `softmax` self-attention operation between all grid points with asymptotic scaling  $\mathcal{O}(N_g^2)$  is prohibitively numerically expensive. For large point cloud datasets like densities  $n(\mathbf{r})$  on Becke grids, this is necessary to avoid materializing the full  $N_g \times N_g$  kernel matrix  $\mathcal{K}(\mathbf{r}_i, \mathbf{r}_j)$ , incurring prohibitively large memory requirements. Instead, in Eq. 2, we first contract  $K(\mathbf{r})$  and  $V(\mathbf{r}')$ , then perform the integral and, finally, multiply by  $Q(\mathbf{r})$ .

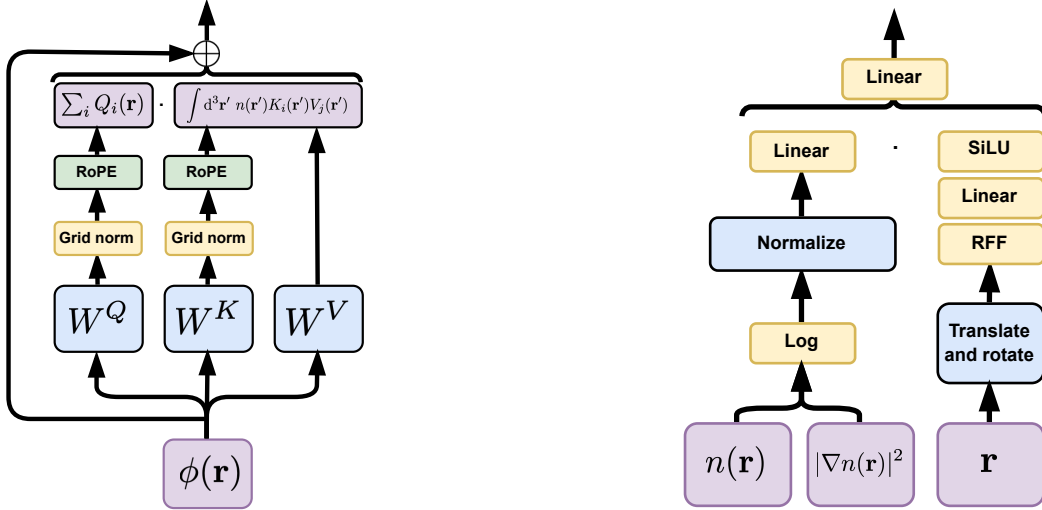


FIG. 1. Diagrammatic representations of internal connectivities of GDA sub-components. **Left:** The linear attention module enabling the nonlocal behavior of resulting functionals. **Right:** The field embedding module lifting the local field representations to a high-dimensional space.

Additionally, we apply custom *grid normalization*, to field projections of the input field  $\phi$  defined in Eq. 3 before performing the attention operation in Eq. 2. Grid normalization amounts to normalizing keys  $K$  and queries  $Q$  in the following way:

$$f(\mathbf{r}) \mapsto \frac{f(\mathbf{r})}{\sqrt{\int d^3\mathbf{r} n(\mathbf{r})(f(\mathbf{r}))^2}}, \quad (5)$$

in an component-wise way for multi-component fields. We note that the choice of leaving values  $V$  unnormalized has been called *Fourier* linear attention as opposed to *Galerkin* linear attention where keys and values are normalized.

Furthermore, in order to ensure that the resulting kernel  $\mathcal{K}(\mathbf{r} - \mathbf{r}') = Q(\mathbf{r}) \cdot K(\mathbf{r}')$  is purely a function of the relative coordinate, we employ rotary positional encoding (RoPE) [4, 5]. The RoPE mechanism relies on the composition property of representations  $D$  of the rotation group  $SO(2)$  in two dimensions:  $D(\alpha)D(\alpha') = D(\alpha + \alpha')$  for angles  $\alpha$  and  $\alpha'$ .

We generalize the RoPE mechanism to three spatial dimensions by setting  $\alpha = \mathbf{k} \cdot \mathbf{r}$  for an input at point  $\mathbf{r} \in \mathbb{R}^3$  and include  $\mathbf{k} \in \mathbb{R}^3$  in the learnable parameters of the model. Therefore, we have

$$D(\mathbf{k} \cdot \mathbf{r})D(-\mathbf{k} \cdot \mathbf{r}') = D(\mathbf{k} \cdot \mathbf{r})D^{-1}(\mathbf{k} \cdot \mathbf{r}') = D(\mathbf{k} \cdot (\mathbf{r} - \mathbf{r}')). \quad (6)$$

To construct an orthogonal representation  $D$  operating on the input field components  $\phi_i(\mathbf{r})$  and exploit Eq. 6, we first note that a trivial representation of  $SU(2)$  on  $\mathbb{R}^2$  is given by simple rotation matrices

$$D_{\mathbb{R}^2}(\alpha) = \begin{bmatrix} \cos \alpha & \sin \alpha \\ -\sin \alpha & \cos \alpha \end{bmatrix}. \quad (7)$$

Therefore, a multi-component input field  $\phi(\mathbf{r})$  with an even number of components, we define the 3D RoPE as a trivially reducible orthogonal representation  $\phi(\mathbf{r}) \mapsto D_{\mathbb{R}^{2n}}(\mathbf{k} \cdot \mathbf{r}) \phi(\mathbf{r})$  with

$$D_{\mathbb{R}^{2n}}(\mathbf{k}_1 \cdot \mathbf{r}, \dots, \mathbf{k}_n \cdot \mathbf{r}) = \begin{bmatrix} \cos(\mathbf{k}_1 \cdot \mathbf{r}) & \sin(\mathbf{k}_1 \cdot \mathbf{r}) & & & & & & & \\ -\sin(\mathbf{k}_1 \cdot \mathbf{r}) & \cos(\mathbf{k}_1 \cdot \mathbf{r}) & & & & & & & \\ & & \ddots & & & & & & \\ & & & \ddots & & & & & \\ & & & & \cos(\mathbf{k}_n \cdot \mathbf{r}) & \sin(\mathbf{k}_n \cdot \mathbf{r}) & & & \\ & & & & -\sin(\mathbf{k}_n \cdot \mathbf{r}) & \cos(\mathbf{k}_n \cdot \mathbf{r}) & & & \\ & & & & & & \ddots & & \\ & & & & & & & \ddots & \\ & & & & & & & & \cos(\mathbf{k}_n \cdot \mathbf{r}) & \sin(\mathbf{k}_n \cdot \mathbf{r}) \\ & & & & & & & & -\sin(\mathbf{k}_n \cdot \mathbf{r}) & \cos(\mathbf{k}_n \cdot \mathbf{r}) \end{bmatrix} \quad (8)$$

depending on  $n$  rotation angles defined by trainable parameters  $\mathbf{K} = \{\mathbf{k}_1, \dots, \mathbf{k}_n\}$ . The block-diagonal structure in Eq. 8 mixes adjacent components of the input field in a way that reflects the target  $SO(2)$  multiplication property. In that case, the query-key product in Eq. 2

$$\begin{aligned} \mathcal{K}(\mathbf{r}, \mathbf{r}') &= Q(\mathbf{r}) \cdot K(\mathbf{r}') = \\ &= [D(\mathbf{K} \cdot \mathbf{r})W^Q \phi(\mathbf{r})]^\top [D(\mathbf{K} \cdot \mathbf{r}')W^K \phi(\mathbf{r})] = \\ &= \phi(\mathbf{r})^\top (W^Q)^\top D^\top (\mathbf{K} \cdot \mathbf{r}) D (\mathbf{K} \cdot \mathbf{r}') W^K \phi(\mathbf{r}) = \\ &= \phi(\mathbf{r})^\top (W^Q)^\top D^\top (-\mathbf{K} \cdot (\mathbf{r} - \mathbf{r}')) W^K \phi(\mathbf{r}) = \\ &= \mathcal{K}(\mathbf{r} - \mathbf{r}') \end{aligned}$$

reduces the linear attention integral to a learnable continuous convolution, if we apply the 3D RoPE transformation as a final step just before integration.

Finally, after the attention layer has been updated, the output field  $\phi$  is transformed by a component-wise gated multi-layer perceptron [6]:

$$\phi(\mathbf{r}) \mapsto W_3 ((W_1 \phi(\mathbf{r}) + \mathbf{b}_1) \odot \sigma(W_2 \phi(\mathbf{r}) + \mathbf{b}_2)) + \mathbf{b}_3 \quad (9)$$

with SiLU activations [7]  $\sigma(x) = \frac{x}{1+e^{-x}}$ . Weights  $W_i$  and biases  $\mathbf{b}_i$  are included in trainable parameters and  $\odot$  indicates element-wise multiplication.

In summary, the steps comprising one GDA *block* are:

1. Evaluate raw queries, keys and values by linear projections in Eq. 3.
2. Normalize queries and keys using grid normalization in Eq. 5.
3. Apply the 3D RoPE transformation in Eq. 8 to queries and keys.
4. Evaluate the final linear attention integral in Eq. 2 using the kernel trick. Add a skip connection.
5. Normalize [8] and apply the gated MLP in Eq. 9. Add a skip connection.

Internal connectivity of sub-layers can be found in Fig. 1.

### Field embedding

The field embedding layer is used in the GDA architecture to ensure correct symmetry properties of the learned model. Since the model is explicitly coordinate-dependent, we fix a coordinate system to perform the computation with comparable values of resulting *computational* coordinates. We choose the coordinate system in which the mean value (electronic dipole moment)

$$\boldsymbol{\mu} = \frac{1}{N} \int d^3\mathbf{r} n(\mathbf{r}) \mathbf{r} \quad (10)$$

vanishes and the covariance matrix

$$\Sigma_{ij} = \frac{1}{N} \int d^3\mathbf{r} n(\mathbf{r}) (r_i - \mu_i) (r_j - \mu_j) \quad (11)$$

is diagonal. After fixing translations and rotations, individual coordinates  $\mathbf{r}_i$  are independently embedded into a  $d$ -dimensional space as

$$\mathbf{r} \mapsto \xi(\mathbf{r}) = \frac{1}{\sqrt{d}} [\cos(K_0 \mathbf{r}) \parallel \sin(K_0 \mathbf{r})]^\top, \quad (12)$$

where  $\parallel$  denotes vector concatenation and  $K_0 \in \mathbb{R}^{\frac{d}{2} \times 3}$  is a trainable matrix randomly initialized with values sampled from the normal distribution  $\mathcal{N}(0, \sigma^{-2})$ . This *random Fourier feature* (RFF) encoding has effectively been used to encode high-frequency maps of continuous coordinates in kernel learning [12], and has been shown to measurably increase expressivity of various architectures in geometric deep learning [13–15], including in combination with transformers [16].

Symbol	Name	Value	Domain	Description
$L$	Number of blocks	3	$\mathbb{N}$	GDA block count
$d$	Field embedding dimension	128	$\mathbb{N}$	Dimension of internal field representations within the model
$\sigma$	RFF kernel scale	1	$\mathbb{R}_+$	Gaussian scale used to initialize the RFF embedding layer
$\eta$	Learning rate	Scheduled $2 \times 10^{-4} \rightarrow 5 \times 10^{-5}$	$\mathbb{R}_+$	(R)Adam optimizer learning rate [9, 10]
$B$	Batch size	288	$\mathbb{N}$	Number of molecules used for cost gradient estimation
$N_e$	Number of epochs	4000	$\mathbb{N}$	Number iterations over the entire dataset
$\lambda$	Relative cost weight	1	$\mathbb{R}_+$	Constant multiplier for the potential matrix penalty in the main text
$\tilde{\lambda}$	Weight decay	0.01	$\mathbb{R}_+$	Weight decay regularizer for the network parameters [11]
$\alpha$	Enhancement	2	$\mathbb{R}_+$	Relative increase in the number of features in the middle MLP layer.
$t_1$	Learning rate annealing start	$N_e/3$	$\mathbb{N}$	Epoch at which the learning rate annealing starts (see Fig. 2)
$t_2$	Learning rate annealing end	$0.95 N_e$	$\mathbb{N}$	Epoch at which the learning rate annealing ends (see Fig. 2)

TABLE I. The list of relevant hyperparameter choices used in this work.

The mapping  $\mathbf{r} \mapsto \xi(\mathbf{r})$  in Eq. 12 is designed to take advantage of the (approximate) kernel trick described in the main text, in a related way to the RoPE mechanism described in Eq. 8. However, we emphasize that it is often used outside the kernel context, as a featurization layer (called *positional encoding*) for coordinate-dependent neural network inputs. Suppose that a convolution integral with a kernel  $\mathcal{K}$  needs evaluation. Denoting Fourier transforms with hats and employing the convolution theorem in combination with Monte Carlo integration, we have:

$$\int d^3\mathbf{r}' \mathcal{K}(\mathbf{r} - \mathbf{r}')f(\mathbf{r}') = \int \frac{d^3\mathbf{k}}{(2\pi)^3} \hat{\mathcal{K}}(\mathbf{k}) \hat{f}(\mathbf{k}) e^{i\mathbf{k}\cdot\mathbf{r}} \approx \frac{1}{(2\pi)^3} \times \frac{1}{N_s} \sum_j \hat{f}(\mathbf{k}_j) e^{i\mathbf{k}_j\cdot\mathbf{r}} \quad (13)$$

for  $N_s$  samples  $\mathbf{k}_j \sim \hat{\mathcal{K}}$ , assuming the the kernel  $\mathcal{K}$  is a positive distribution on both sides of the Fourier transform. Therefore, the spread of the distribution in determines the initialization of  $K_0$  and it is, in turn, determined by the inverse of the spread of  $\mathcal{K}$  in real space, constrained by the uncertainty relation. If we choose to initialize the kernel as a Gaussian  $\mathcal{N}$ , we have  $\mathbf{k}_j \sim \exp(-\frac{1}{2}\sigma^2\mathbf{k}^2) \propto \mathcal{N}(0, \sigma^{-2})$ .

Local density field values are embedded into a  $d$ -dimensional space as well with learnable linear projections of normalized values. We take local field information in the form of  $n(\mathbf{r})$  and  $\gamma(\mathbf{r}) = |\nabla n(\mathbf{r})|^2$  and construct

$$\overline{\ln n(\mathbf{r})} = \frac{\ln n(\mathbf{r}) - \langle \ln n(\mathbf{r}) \rangle}{\sqrt{\langle (\ln n(\mathbf{r}) - \langle \ln n(\mathbf{r}) \rangle)^2 \rangle}} \quad \text{and} \quad \overline{\ln \gamma(\mathbf{r})} = \frac{\ln \gamma(\mathbf{r}) - \langle \ln \gamma(\mathbf{r}) \rangle}{\sqrt{\langle (\ln \gamma(\mathbf{r}) - \langle \ln \gamma(\mathbf{r}) \rangle)^2 \rangle}}, \quad (14)$$

where we use the density average  $\langle \cdot \rangle = \frac{1}{N} \int d^3\mathbf{r}' n(\mathbf{r}')(\cdot)$ , normalized to unity. In practice, we initialize

$$\phi(\mathbf{r}) = W^E \left[ \frac{\ln(n(\mathbf{r}) + \epsilon)}{\ln(\gamma(\mathbf{r}) + \epsilon)} \right] \quad (15)$$

with  $\epsilon = 10^{-4}$ , instead of bare logarithms for numerical stability and  $W^E \in \mathbb{R}^{d \times 2}$  are trainable parameters represented by trainable unit vectors in the main text. After input fields and coordinates have been independently processed, we combine them using learnable weights  $W$  and biases  $b$

$$\phi(\mathbf{r}) \mapsto W'(\phi(\mathbf{r}) \odot \sigma(W^\xi \xi(\mathbf{r}) + b^\xi)) + b' . \quad (16)$$

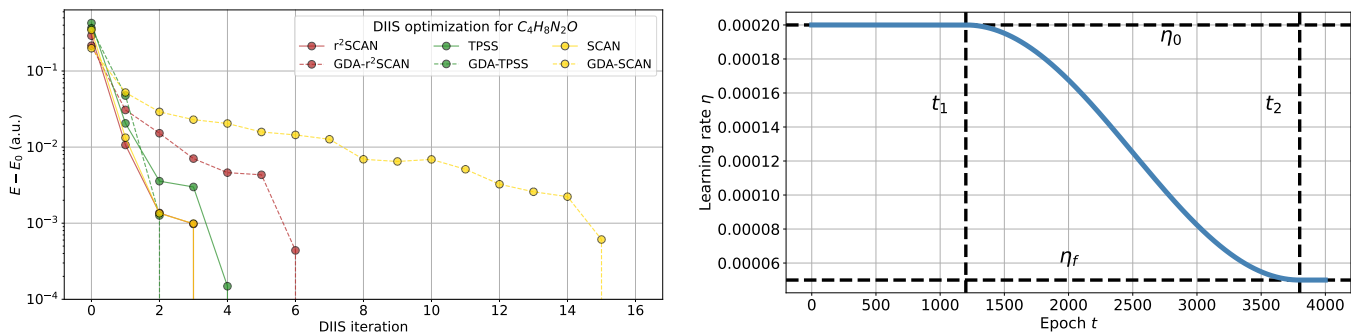


FIG. 2. Convergence properties of the GDA functionals. **Left:** Convergence properties of the DIIS [17] optimization used in PySCF [18, 19], on an example of a random molecule from the test dataset. **Right:** The learning rate scheduling used to optimize the full GDA model.

to produce final density embeddings. We use  $\sigma = \text{SiLU}$  as an element-wise nonlinear activation function [7]. A list of all relevant hyperparameters used in this work can be found in table . A diagram of the overall connectivity of the embedding layer can be found in the right panel of Fig. 1.

## OPTIMIZATION AND CONVERGENCE

### Neural-network training

As noted in the main text, the GDA neural network was trained with  $L = 3$  blocks, internal field embedding dimension  $d = 128$ , totaling 645000 parameters. The rectified Adam [9] (RAdam) [10] optimizer was used for  $N_e = 4000$  epochs with learning rate decreasing from  $\eta_i = 2 \times 10^{-4}$  to  $\eta_f = 5 \times 10^{-5}$  using a customized cosine annealing schedule defined as

$$\eta_t = \begin{cases} \eta_i, & \text{if } t < t_1 \\ \eta_f + (\eta_i - \eta_f) \cos^2\left(\frac{\pi}{2} \frac{t - t_1}{t_2 - t_1}\right), & \text{if } t_1 \leq t \leq t_2 \\ \eta_f, & \text{if } t > t_2 \end{cases} \quad (17)$$

for epoch  $t$ . The schedule is shown in Fig. 2. We find that decreasing the learning rate during the course of training helps fine-tune the model in the later epochs when the loss landscape changes at smaller scales. We set  $t_1 = N_e/3$  and  $t_2 = 0.95N_e$ .

### Self-consistent field optimization from first principles

We use PySCF [18, 19] for first-principles optimizations of molecular densities, where the default method is the standard SCF Pulay mixing or direct inversion in the iterative subspace (DIIS) [17]. Using that method, we optimize a random molecule from the training dataset a total of six times – three times with library [20] versions of targeted MGGA functionals [21–23] and three times with the GDA substitution  $\tau \rightarrow \tau_\theta$ . Results can be seen in the left panel of Fig. 2.

We note that r<sup>2</sup>SCAN and TPSS converge in a similar number of mixing iterations as the original functionals while SCAN (included for comparison) appears to be more sensitive to numerical noise stemming from the GDA approximation. We report that this trend persists in most other molecules we have examined more closely.

## DENSITY FUNCTIONAL THEORY

### Kohn-Sham density functional theory

As set up in the main text, we consider isolated molecular systems. A DFT calculation [24] outputs an approximation to the ground state density  $n_0$  minimizing the total energy:  $n_0(\mathbf{r}) = \operatorname{argmin}_n E[n]$  where

$$E[n] = T[n] + E_{\text{ext}}[n] + E_H[n] + E_{\text{xc}}[n] \quad (18)$$

Known terms in the total energy functional  $E[n]$  given in Eq. 18 are the external contribution  $E_{\text{ext}}[n]$

$$E_{\text{ext}}[n] = \int d^3\mathbf{r} n(\mathbf{r}) v_{\text{ext}}(\mathbf{r}) \quad (19)$$

capturing the effects of the atomic Coulomb interaction  $v_{\text{ext}}(\mathbf{r})$  and the direct Hartree component capturing the classical electronic Coulomb interaction:

$$E_H[n] = \frac{1}{2} \int d^3\mathbf{r} \int d^3\mathbf{r}' \frac{n(\mathbf{r})n(\mathbf{r}')}{|\mathbf{r} - \mathbf{r}'|}. \quad (20)$$

Kohn-Sham DFT [25] framework assumes that the density  $n_0$  comes from an effective system of non-interacting electrons with orbitals  $\Psi = \{\psi_k(\mathbf{r}) \mid k = 1, \dots, N\}$  where  $N$  is the number of electrons in the system. In that case, the kinetic term in Eq. 18 evaluates to

$$T[n] \mapsto T_{\text{KS}}[n] = \sum_a n_a \int d^3\mathbf{r} \psi_a^*(\mathbf{r}) \left( -\frac{1}{2} \nabla^2 \right) \psi_a(\mathbf{r}) = \frac{1}{2} \sum_a n_a \int d^3\mathbf{r} |\nabla \psi_a(\mathbf{r})|^2. \quad (21)$$

After the desired kinetic and XC functional has been specified, the constrained minimization of the total energy functional given in Eq. 18 can proceed, enforcing orbital normalization with Lagrange multipliers  $\epsilon_a$ :

$$\mathcal{L}[\Psi] = E[\Psi] + \sum_a \epsilon_a \int d^3\mathbf{r} |\psi_a(\mathbf{r})|^2 = T_{\text{KS}}[\Psi] + U[\Psi] + \sum_a \epsilon_a \int d^3\mathbf{r} |\psi_a(\mathbf{r})|^2 \quad (22)$$

where we choose to trivially rewrite all density functionals as orbital functionals and collect all of the different kinds of potential energy into  $U[\Psi] = E_{\text{ext}}[\Psi] + E_H[\Psi] + E_{\text{xc}}[\Psi]$ . Trivial functional differentiation yields:

$$\frac{\delta \mathcal{L}[\Psi]}{\delta \psi_a^*(\mathbf{r})} = \left( -\frac{1}{2} \nabla^2 + v_{\text{eff}}[n](\mathbf{r}) - \epsilon_a \right) \psi_a(\mathbf{r}) \implies \left( -\frac{1}{2} \nabla^2 + v_{\text{eff}}[n](\mathbf{r}) \right) \psi_a(\mathbf{r}) = \epsilon_a \psi_a(\mathbf{r}), \quad (23)$$

known as the Kohn-Sham (KS) equation. Mathematically speaking, the KS Eq. 23 is a non-linear partial differential equation for the unknown orbitals  $\Psi$ . The source of non-linearity, other than the classical Coulomb term, comes from exchange and correlation effects built into the approximate functional  $E_{\text{xc}}$  that gives rise to the effective one-electron potential

$$v_{\text{eff}}(\mathbf{r}) = \frac{\delta U[n]}{\delta n(\mathbf{r})} = v_{\text{ext}}(\mathbf{r}) + \int d^3\mathbf{r}' \frac{n(\mathbf{r}')}{|\mathbf{r} - \mathbf{r}'|} + \frac{\delta E_{\text{xc}}[n]}{\delta n(\mathbf{r})}. \quad (24)$$

The last term in Eq. 24 is sometimes labeled as the XC potential  $v_{\text{xc}}(\mathbf{r})$  and in it highlights the importance of being able to calculate functional derivatives of the XC functional efficiently.

Numerically, Eq. 23 is usually solved in a self-consistent (SCF) manner, ensuring that  $n(\mathbf{r}) = \sum_a n_a |\psi_a(\mathbf{r})|^2$ . The SCF procedure takes the form of fixed-point iteration of the following two steps, starting from the initial guess for  $n(\mathbf{r})$ :

- Update orbital estimates  $\Psi$  by solving Eq. 23 for a fixed density.
- Update density estimate through  $n(\mathbf{r}) = \sum_a n_a |\psi_a(\mathbf{r})|^2$ .

The loop is terminated after successive density and energy estimates stop changing beyond a given tolerance.

### Calculations in the basis of atomic orbitals

For isolated molecular systems, Gaussian basis sets are a common approach of representing atomic orbitals used in density expansions. In this subsection, we derive all of the expressions used during training to evaluate the GDA effective one-particle Hamiltonian

$$H_{\text{eff}} = \frac{\mathbf{p}^2}{2} + v_{\text{eff}}[n](\mathbf{r}) \quad (25)$$

from the neural-network functional using automatic differentiation, with  $\mathbf{p}$  being the one-particle momentum operator. With the definition of Eq. 25, the KS equations simply read  $H_{\text{eff}}|\psi_a\rangle = \epsilon_a|\psi_a\rangle$ .

In the following, we use Greek indices  $\{\mu, \nu, \dots\}$  for the fixed atomic orbital (AO) basis and latin  $\{a, b, \dots\}$  indices for the molecular orbital (MO) basis. The two bases are related by the LCAO (linear combination of atomic orbitals) coefficients  $C$  as  $|\psi_a\rangle = \sum_{\mu} C_{\mu a} |\chi_{\mu}\rangle$ . The density matrix  $\Gamma$  is usually defined in the AO basis through

$$n(\mathbf{r}) = \sum_{\mu\nu} \Gamma_{\mu\nu} \chi_{\mu}(\mathbf{r}) \chi_{\nu}(\mathbf{r}) . \quad (26)$$

The full effective Hamiltonian matrix in the AO basis decomposes as:

$$F_{\mu\nu} = \langle \chi_{\mu} | H_{\text{eff}} | \chi_{\nu} \rangle = \frac{\partial E}{\partial \Gamma_{\mu\nu}} = T_{\mu\nu} + V_{\mu\nu} + J_{\mu\nu} + X_{\mu\nu} , \quad (27)$$

where  $T$ ,  $V$ ,  $J$ , and  $X$  are kinetic, nuclear, Coulomb and XC matrices, respectively. These quantities are readily available in quantum chemistry software packages and we save  $T$  as a part of the training dataset. The Kohn-Sham kinetic energy functional is of special interest in this work. Employing partial integration, we get

$$\begin{aligned} T[n] &= \sum_a n_a \langle \psi_a | \frac{\mathbf{p}^2}{2} | \psi_a \rangle = \\ &= \sum_a n_a \int d^3\mathbf{r} \psi_a^*(\mathbf{r}) \left( -\frac{1}{2} \nabla^2 \right) \psi_a(\mathbf{r}) = \frac{1}{2} \sum_a n_a \int d^3\mathbf{r} |\nabla \psi_a(\mathbf{r})|^2 = \\ &= \sum_{\mu\nu} \left( \sum_a n_a C_{\mu a} C_{\nu a} \right) \times \frac{1}{2} \int d^3\mathbf{r} \nabla \chi_{\mu}(\mathbf{r}) \cdot \nabla \chi_{\nu}(\mathbf{r}) = \sum_{\mu\nu} \Gamma_{\mu\nu} T_{\mu\nu} = \text{Tr}(\Gamma T) , \end{aligned}$$

where we identify the kinetic energy matrix  $T_{\mu\nu}$  that goes into the cost function defined in the main text. Other similar matrices in the AO basis work out to be:

$$\begin{aligned} T_{\mu\nu} &= \frac{1}{2} \int d^3\mathbf{r} \nabla \chi_{\mu}(\mathbf{r}) \cdot \nabla \chi_{\nu}(\mathbf{r}) , \quad V_{\mu\nu} = \int d^3\mathbf{r} v_{\text{ext}}(\mathbf{r}) \chi_{\mu}(\mathbf{r}) \chi_{\nu}(\mathbf{r}) \quad \text{and} \\ J_{\mu\nu} &= \sum_{\alpha\beta} \Gamma_{\alpha\beta} \int d^3\mathbf{r} \int d^3\mathbf{r}' \frac{\chi_{\mu}(\mathbf{r}) \chi_{\nu}(\mathbf{r}) \chi_{\alpha}(\mathbf{r}') \chi_{\beta}(\mathbf{r}')}{|\mathbf{r} - \mathbf{r}'|} . \end{aligned} \quad (28)$$

The XC matrix  $X$  is the only component we need to evaluate using from the GDA functional in order to regularize the training loop. We only need to evaluate the derivative of the total XC energy with respect to the input density matrix because:

$$\hat{X}_{\mu\nu} = \frac{\partial \hat{E}_{\text{xc}}}{\partial \Gamma_{\mu\nu}} = \int d^3\mathbf{r} \frac{\delta \hat{E}_{\text{xc}}}{\delta n(\mathbf{r})} \frac{\partial n(\mathbf{r})}{\partial \Gamma_{\mu\nu}} = \int d^3\mathbf{r} \hat{v}_{\text{xc}}(\mathbf{r}) \chi_{\mu}(\mathbf{r}) \chi_{\nu}(\mathbf{r}) . \quad (29)$$

where we put hats on quantities estimated using the GDA functional approximation. These derivatives can be calculated efficiently using automatic differentiation at the cost of evaluating the functional itself.

---

\* [mmedvidovic@ethz.ch](mailto:mmedvidovic@ethz.ch)

[1] S. Cao, *Choose a Transformer: Fourier or Galerkin* (2021), arXiv:2105.14995 [cs, math], URL <http://arxiv.org/abs/2105.14995>.

- [2] A. Vaswani, N. Shazeer, N. Parmar, J. Uszkoreit, L. Jones, A. N. Gomez, L. Kaiser, and I. Polosukhin (2017), arXiv: 1706.03762, URL <http://arxiv.org/abs/1706.03762>.
- [3] A. Dosovitskiy, L. Beyer, A. Kolesnikov, D. Weissenborn, X. Zhai, T. Unterthiner, M. Dehghani, M. Minderer, G. Heigold, S. Gelly, et al. (2020), arXiv: 2010.11929, URL <http://arxiv.org/abs/2010.11929>.
- [4] J. Su, Y. Lu, S. Pan, A. Murtadha, B. Wen, and Y. Liu, *RoFormer: Enhanced Transformer with Rotary Position Embedding* (2023), arXiv:2104.09864 [cs], URL <http://arxiv.org/abs/2104.09864>.
- [5] Z. Li, K. Meidani, and A. B. Farimani, *Transformer for Partial Differential Equations' Operator Learning* (2023), arXiv:2205.13671 [cs], URL <http://arxiv.org/abs/2205.13671>.
- [6] N. Shazeer, *GLU Variants Improve Transformer* (2020), URL <https://arxiv.org/abs/2002.05202v1>.
- [7] S. Eklund, E. Uchibe, and K. Doya (2017), arXiv: 1702.03118, URL <http://arxiv.org/abs/1702.03118>.
- [8] J. L. Ba, J. R. Kiros, and G. E. Hinton (2016), arXiv: 1607.06450, URL <http://arxiv.org/abs/1607.06450>.
- [9] D. P. Kingma and J. L. Ba, in *3rd International Conference on Learning Representations, ICLR 2015 - Conference Track Proceedings* (International Conference on Learning Representations, ICLR, 2015).
- [10] L. Liu, H. Jiang, P. He, W. Chen, X. Liu, J. Gao, and J. Han (2019), arXiv: 1908.03265, URL <http://arxiv.org/abs/1908.03265>.
- [11] I. Loshchilov and F. Hutter, CoRR **abs/1711.05101** (2017), arXiv: 1711.05101, URL <http://arxiv.org/abs/1711.05101>.
- [12] A. Rahimi and B. Recht, in *Advances in Neural Information Processing Systems*, edited by J. Platt, D. Koller, Y. Singer, and S. Roweis (Curran Associates, Inc., 2007), vol. 20, URL [https://proceedings.neurips.cc/paper\\_files/paper/2007/file/013a006f03dbc5392effeb8f18fda755-Paper.pdf](https://proceedings.neurips.cc/paper_files/paper/2007/file/013a006f03dbc5392effeb8f18fda755-Paper.pdf).
- [13] B. Mildenhall, P. P. Srinivasan, M. Tancik, J. T. Barron, R. Ramamoorthi, and R. Ng (2020), arXiv: 2003.08934.
- [14] K. Gao, Y. Gao, H. He, D. Lu, L. Xu, and J. Li (2022), arXiv: 2210.00379.
- [15] J. Zheng, S. Ramasinghe, and S. Lucey (2021), arXiv: 2107.02561, URL <http://arxiv.org/abs/2107.02561>.
- [16] Y. Li, S. Si, G. Li, C.-J. Hsieh, and S. Bengio (2021), arXiv: 2106.02795, URL <http://arxiv.org/abs/2106.02795>.
- [17] P. Pulay, *Chemical Physics Letters* **73**, 393 (1980), ISSN 00092614, URL <https://linkinghub.elsevier.com/retrieve/pii/0009261480803964>.
- [18] Q. Sun, T. C. Berkelbach, N. S. Blunt, G. H. Booth, S. Guo, Z. Li, J. Liu, J. D. McClain, E. R. Sayfutyarova, S. Sharma, et al., *WIREs Computational Molecular Science* **8**, e1340 (2018), URL <https://wires.onlinelibrary.wiley.com/doi/abs/10.1002/wcms.1340>.
- [19] Q. Sun, X. Zhang, S. Banerjee, P. Bao, M. Barbry, N. S. Blunt, N. A. Bogdanov, G. H. Booth, J. Chen, Z.-H. Cui, et al., *The Journal of Chemical Physics* **153**, 024109 (2020), ISSN 0021-9606, URL <https://doi.org/10.1063/5.0006074>.
- [20] M. A. Marques, M. J. Oliveira, and T. Burnus, *Computer Physics Communications* **183**, 2272 (2012), ISSN 00104655, URL <https://linkinghub.elsevier.com/retrieve/pii/S0010465512001750>.
- [21] J. Sun, R. C. Remsing, Y. Zhang, Z. Sun, A. Ruzsinszky, H. Peng, Z. Yang, A. Paul, U. Waghmare, X. Wu, et al. (2015), arXiv: 1511.01089, URL <http://arxiv.org/abs/1511.01089>.
- [22] J. W. Furness, A. D. Kaplan, J. Ning, J. P. Perdew, and J. Sun, *The Journal of Physical Chemistry Letters* **11**, 8208 (2020), ISSN 1948-7185, 1948-7185, URL <https://pubs.acs.org/doi/10.1021/acs.jpclett.0c02405>.
- [23] J. Tao, J. P. Perdew, V. N. Staroverov, and G. E. Scuseria, *Physical Review Letters* **91**, 146401 (2003), ISSN 0031-9007, 1079-7114, URL <https://link.aps.org/doi/10.1103/PhysRevLett.91.146401>.
- [24] R. M. Martin, *Electronic structure: basic theory and practical methods* (Cambridge university press, 2020).
- [25] W. Kohn and L. J. Sham, *Physical Review* **140**, A1133 (1965), ISSN 0031-899X, URL <https://link.aps.org/doi/10.1103/PhysRev.140.A1133>.